

# First Principles Calculations of the Effect of Stress in the I-V Characteristics of the CoSi<sub>2</sub>/Si Interface

Oscar D. Restrepo, Qun Gao, Shesh M. Pandey, Eduardo Cruz-Silva, El Mehdi Bazizi  
GLOBALFOUNDRIES  
Malta, NY, 12020, USA  
oscar.restrepo@globalfoundries.com

**Abstract**—We present *ab initio*-based electronic transport calculations on the effect of uniaxial and bi-axial stress on the CoSi<sub>2</sub>/nSi interface resistivity for the three main silicon crystallographic directions. For the [001] case, we identify two distinctive low and high bias conduction regimes for both compressive and tensile stress. In these regimes, the current is dominated by electronic transmission pathways near the  $\Gamma$  point for bias up to  $\sim 0.1V$ , while for higher bias it is dominated by transmission at the  $(\pm 1/2, \pm 1/2)$  conduction band valleys of the Brillouin zone, which results in a contact resistivity decrease of up to 30% at 0.2V bias. This effect is less pronounced for the [110] direction, and negligible for the [111] case due to the symmetry of the Si conduction band valleys along these directions. This study provides insight into stress-based optimization pathways for contact resistivity reduction of silicide interfaces in next generation semiconductor devices.

**Keywords**—*Ab initio*, electronic transport, silicide, contact resistivity

## I. INTRODUCTION

With the continuous aggressive channel scaling of modern metal-oxide-semiconductor field effect transistors (MOSFET) devices, parasitic resistances have become the dominant component in the MOSFET on-resistance and have a strong impact on the device performance limit. Among these, contact resistance plays an increasingly important role on restricting the device performance [1], hence considerable research efforts have been focused on reducing the silicide/silicon contact resistivity [2-4]. Transport across the epitaxial silicide/silicon interface (Fig. 1) has unique interesting properties that differentiate it from bulk transport and makes engineering of its transport properties more challenging. The valley filtering effect in transport behavior of CoSi<sub>2</sub>/Si interface was first reported by Gao and Guo [5] and was identified as a strong limiting factor to contact resistivity. Weber [6] and Hegde et al. [7] further performed a comprehensive study for this valley filtering effect, exploring surface orientation and transverse boundary conditions. In this paper, we explore the electronic transport behavior of CoSi<sub>2</sub>/nSi interface under stress with a full *ab initio* methodology, that includes full atomistic relaxation at the interface, and provide insight into engineering opportunities for using stressed materials to optimize the interface transport.

## II. METHODOLOGY

We prepared CoSi<sub>2</sub>/Si interfaces (Fig. 2) with their transport direction oriented along their [001] crystallographic direction. The periodic axes for the normal plane are defined along the [110] and  $[1-10]$  directions, and CoSi<sub>2</sub> was allowed to expand to account for a lattice mismatch of 1.5%. The interface structure was created by attaching a 20 Å layer of CoSi<sub>2</sub> to a 42 Å layer of Si. These, in turn, are connected to semi-infinite electrodes of 10.3 Å of CoSi<sub>2</sub> on the left side and 10.7 Å of Si on the right side. A typical supercell has a tetragonal structure with lattice parameter  $a \approx 3.8$  Å.

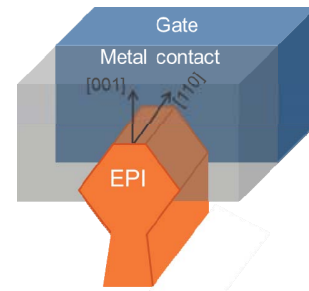


Fig 1: Schematic of source/drain contacts on finFET CMOS devices.

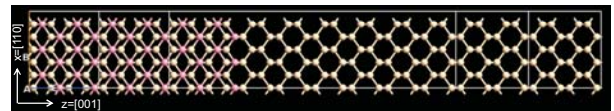


Fig 2. CoSi<sub>2</sub>/Si[001] interface structure.

We used Synopsys QuantumATK v2017.12 to perform *ab initio* non-equilibrium Green's functions (NEGF) transport calculations [8-9] in order to account for the bias voltage at the contact. We use the local spin density approximation (LSDA) to account for exchange and correlation, norm-conserving pseudopotentials are used to represent the atomic nuclei and core electrons, while the wavefunctions are expanded on a double zeta basis set with polarization orbitals (DZP). The k-point mesh for momentum-space integrals consisted of a 22x22x120 Monkhorst-Pack grid, while real-space integrals were sampled on a mesh with a density equivalent to a plane wave energy cutoff of 90 Hartree. Throughout all our calculations, we keep the silicon carrier concentration fixed at

$n=10^{21}$  e/cm<sup>3</sup> by adding a background compensation charge to the atoms on the silicon side of our interface model, as implemented in QuantumATK.

### III. RESULTS

We start by computing the momentum-resolved transmission spectrum of Si and CoSi<sub>2</sub> bulk systems under tensile and compressive stress along the [001] direction. We first relax the silicon lattice to match the target stresses, while CoSi<sub>2</sub> is forced to match the silicon substrate, but allowed to relax in the transport direction. As it can be observed in Fig. 3, 1<sup>st</sup> row the Si conduction band  $\Gamma$ -X and  $\Gamma$ -Y valleys located near the ( $k_A=\pm 1/2$ ,  $k_B=\pm 1/2$ ) points, as well as the  $\Gamma$ -Z valley which is projected around the  $\Gamma$  point of the 2D Brillouin zone dominate Si transmission for all the stresses considered. In

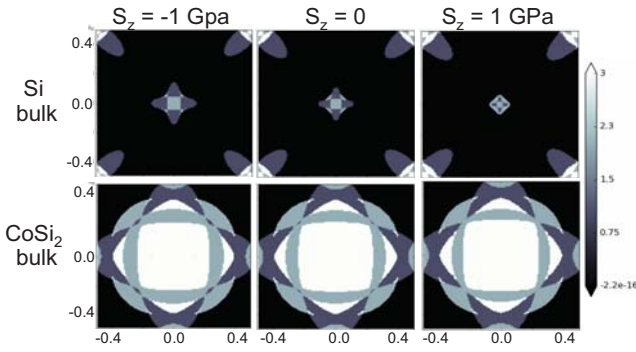


Fig. 3: Si bulk and CoSi<sub>2</sub> bulk transmission spectra for  $S_z = -1, 0$ , and 1 GPa.

contrast, the CoSi<sub>2</sub> band structure does not have these valleys, and the transmission is higher around the  $\Gamma$  point, while vanishing near the corners of the Brillouin zone. Without bias, the  $\Gamma$ -X and  $\Gamma$ -Y valleys are completely filtered in the CoSi<sub>2</sub>/Si interface transmission (see Fig. 4, 1<sup>st</sup> row), and the transmission for both tensile and compressive stress are

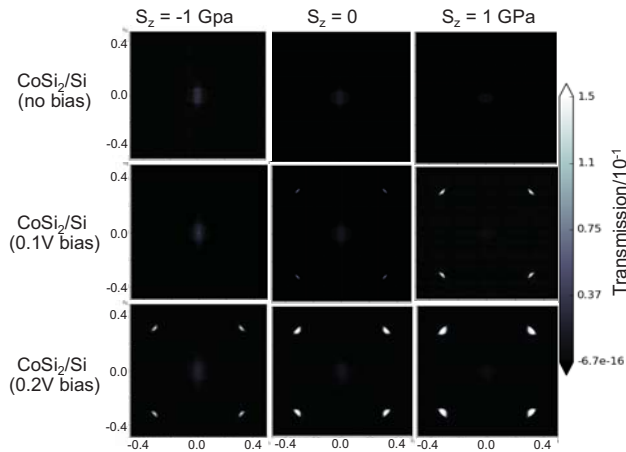


Fig. 4: CoSi<sub>2</sub>/Si transmission spectra for  $S_z = -1, 0$ , and 1 GPa at 0.1 and 0.2 V bias.

dominated by the Fermi surface near the  $\Gamma$  point, showing increased transmission for larger compressions (negative  $S_z$ ) along the [001] direction. As bias voltage is applied, states nearby the valleys become accessible for transmission. The  $\Gamma$ -X valleys are not filtered anymore and start appearing in the transmission spectrum of the CoSi<sub>2</sub>/Si interface (Fig. 4, 2<sup>nd</sup> and 3<sup>rd</sup> rows), eventually dominating the transmission. In this case the transmission becomes larger for higher tensile stress along [001].

The current as a function of bias is plotted in Fig. 5a. We distinguish two bias regimes for both compressive and tensile stresses. For tensile stress we see a crossover from a  $\Gamma$  dominated regime to a  $\Gamma$ -X valley dominated regime at around 0.05 V. For compressive stress the same transition occurs at higher bias ( $\sim 0.11$  V). To understand the origin of this

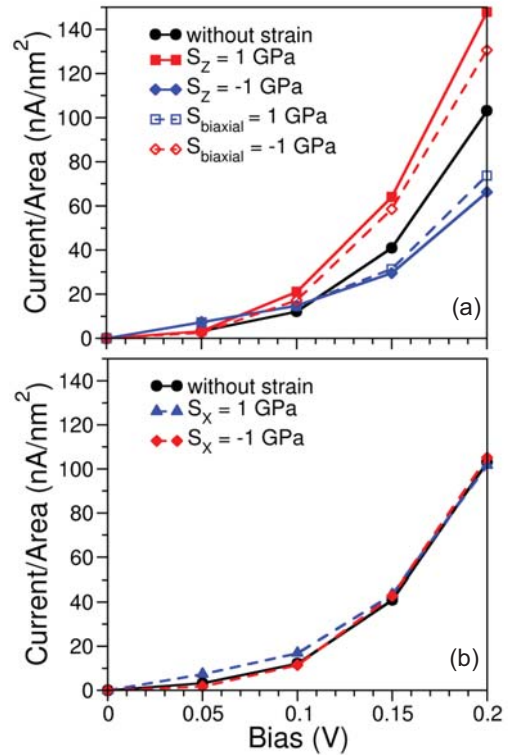


Fig. 5: I-V curves for CoSi<sub>2</sub>/Si interfaces. a) uniaxial along [001] direction and biaxial along transverse directions b) uniaxial along [110] direction.

crossover we have plotted in Fig. 6 the projected density of states in real space as a function of transport direction and energy for a 0.2 V bias. This effectively provides a real space representation of the energy bands. Because of applied bias, there are two Fermi energies ( $E_F$ ) present in the system, one for the metal electrode ( $E_F(\text{metal})$ ) and the other for the semiconductor electrode ( $E_F(\text{semi})$ ). As higher bias is applied more electrons from the metal side will flow to the semiconductor side. As seen in Fig. 6, the electrons moving out of the metal side of the interface at  $E_F(\text{metal})$  will match

empty bands at the semiconductor side with higher energy than  $E_F(\text{semi})$ . These empty bands at higher energies in the semiconductor side have larger Brillouin zone  $\Gamma$ -X valleys than bands closer to  $E_F(\text{semi})$ . This explains the appearance of the valleys in Fig. 4 even if there is no direct overlap at  $E_F(\text{semi})$ , and their dominance at large biases.

Additionally, we confirmed that any stress that effectively results in a lattice expansion of silicon in the transport axis will provide a similar benefit for contact resistivity. By applying uniaxial stress to Si in the  $[110]$  direction  $S_x$  (Fig. 5b), we also observe crossovers in the current vs bias curve but for biases larger than 0.15 V. In this case, for biases lower than 0.15 V, tensile stress in the uniaxial  $[110]$  direction leads to a larger current than compressive stress. This behavior is reverted for biases larger than 0.15 V. Similar I-V characteristics occur when we compare biaxial compressive (tensile) stress in the transverse direction with tensile (compressive) stress in the z-direction (Fig. 5a).

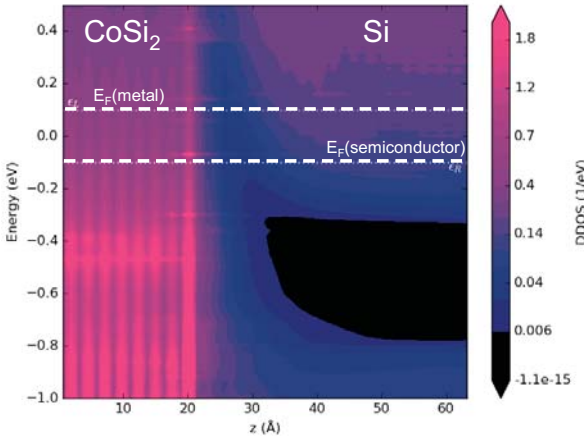


Fig. 6: Projected Density of States of the  $\text{CoSi}_2/\text{Si}$  interface at 0.2V bias.

As the observed stress response of the  $\text{CoSi}_2/\text{Si}$  contact resistivity is due to the momentum-space alignment of the silicon and  $\text{CoSi}_2$  band structures, it is important to assess the effect in other crystallographic directions, namely  $[110]$  and  $[111]$ , as these are commonplace in source and drain contacts in modern finFET CMOS technologies. For this analysis, we performed interface coordinate optimization under the same calculation conditions, but we relaxed our basis set to a single-zeta basis with polarization orbitals for electronic transmission calculations. This reduced basis set represents an acceptable compromise between calculation speed and qualitative accuracy.

Similar to the  $[001]$  direction, the  $\text{CoSi}_2$  transmission in the  $[110]$  and  $[111]$  directions is dominated by states nearby the  $\Gamma$  point, with very little response to the biaxial stress resulting from matching the lattice parameter of the silicon substrate. For the  $[110]$  direction, silicon also displays effects as a result of the applied stress, as seen in figure 7. The  $\Gamma$ -X and  $\Gamma$ -Y valleys remain equivalent by symmetry and are projected nearby the ( $k_A=\pm 1/2, k_B=0$ ) points, while the  $\Gamma$ -Z

valleys are projected nearby the  $\Gamma$  point. The later have a considerable response to the applied stress, as observed on the top row of figure 7. The  $\Gamma$ -Z valley expands (contracts) its

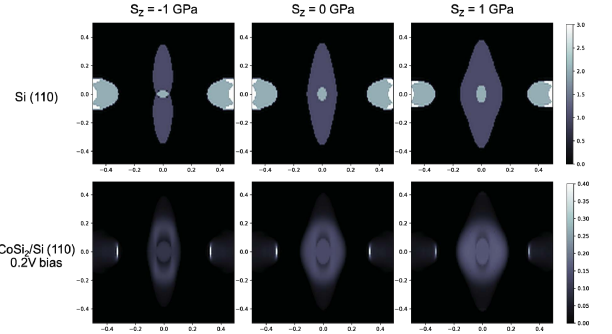


Fig. 7: Stress response of the transmission spectra at  $E_F$  for bulk Si (top) and  $\text{CoSi}_2/\text{Si}$  interface (bottom) oriented along the  $[110]$  direction.

momentum space dispersion as a response to tensile (compressive) stress along the  $[110]$  direction. This change in silicon is carried by the transmission spectrum of the  $\text{CoSi}_2/\text{Si}$  interface, as observed in the bottom row of figure 7. This modulation of the transmission results in a contact resistivity reduction of up to 15% at 0.2 V bias for 1 GPa tensile stress.

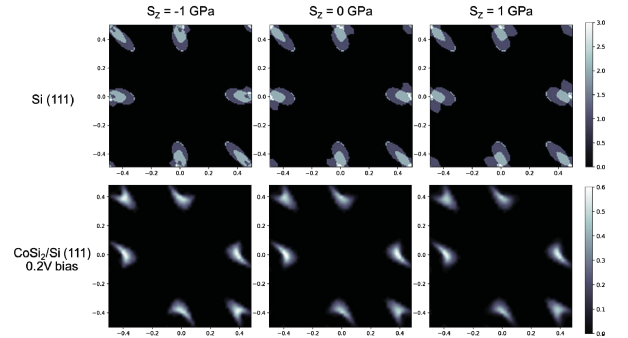


Fig. 8: Stress response of the transmission spectra at  $E_F$  for bulk Si (top) and  $\text{CoSi}_2/\text{Si}$  interface (bottom) oriented along the  $[111]$  direction.

The  $[111]$  direction represents a special case in silicon, as for this transport direction the six conduction band valleys remain equivalent by symmetry. When stress is applied along the  $[111]$  direction all valleys have the same response, and therefore there are no major changes in the silicon transmission spectra, as presented on the top row of figure 8. This stability with respect to stress also translates to the  $\text{CoSi}_2/\text{Si}$  interface, for which we observe that the interface transmission spectra are also near-constant as a function of stress, as shown in the bottom row of figure 8. Consequently, contact resistivity has not only a very modest modulation with stress, it also has an opposite direction when compared with the  $[110]$  and  $[001]$  cases. This reverse trend can be explained by the local changes in the chemical bonding at the interface,

in which compression favors an increased overlap between silicon and  $\text{CoSi}_2$  orbitals, while tensile stress reduces the coupling at the interface. In the absence of changes in the momentum-space distribution of the transmission, these small chemical changes dominate the stress response, and result in a resistivity increase of about 2% for  $S_z=1$  GPa, and a reduction of 3.5% for the compressive stress case of  $S_z=-1$  GPa.

#### IV. CONCLUSION

We have presented a detailed account of the physical factors that result in reduced contact resistivity on  $\text{CoSi}_2/\text{Si}$  interfaces as a function of semiconductor stress and interface crystalline orientation. For the [001] direction, we identified two transmission regimes, at low biases ( $\sim 0.1$  V) the bands centered at  $\Gamma$  dominate the transport, while for larger biases ( $> 0.1$  V) the  $\Gamma$ -X valleys become dominant. We also find that stresses that lead to a lattice expansion of silicon along [001] will result in a reduction of the contact resistivity by as much as 30 % at 0.2 V bias. For the [110] direction, only the  $\Gamma$ -Z valleys are modulated by stress, resulting in a more modest although still significant resistivity reduction of up to 15%. In contrast, the [111] direction shows a negligible resistivity response to stress along the transport direction, highlighting the roles that symmetry breaking and the splitting of the conduction band have on the stress modulation of contact resistivity.

#### REFERENCES

- [1] S.D. Kim, "Optimum location of silicide/Si interface in ultra-thin body SOI MOSFET's with recessed and elevated silicide source/drain contact structure," *Solid State Electron.*, vol. 53(10), pp. 1112-1115, October 2009.
- [2] R. T. Tung, "Recent advances in Schottky barrier concepts," *Mater. Sci. Eng. R.*, vol. 35(1-3), pp. 1-138, November 2001.
- [3] Z. Zhen, Q. Zhijun, L. Ran, M. Ostling, and Z. Shi-Li, "Schottky-Barrier height tuning by means of ion implantation into preformed silicide films followed by drive-in anneal," *IEEE Electron Device Lett.*, vol. 28(7), pp. 565-568, July 2007.
- [4] M. Tao, D. Udeshi, N. Basit, E. Maldonado, and W. P. Kirk, "Removal of dangling bonds and surface states on silicon (001) with a monolayer of selenium," *Appl. Phys. Lett.*, vol. 82(10), p. 1559, March 2003.
- [5] Q. Gao and J. Guo, "Ab initio quantum transport simulation of silicide-silicon contacts," *J. Appl. Phys.*, vol. 111, p. 014305, January 2012.
- [6] C. Weber, "The importance of metal transverse momentum for silicon contact resistivity," *Appl. Phys. Lett.*, vol. 103, p. 193505, November 2013.
- [7] G. Hegde and R. Bowen, "Effect of realistic metal electronic structure on the lower limit of contact resistivity of epitaxial metal-semiconductor contacts," *Appl. Phys. Lett.*, vol. 105, p. 053511, July 2014.
- [8] M. Brandbyge, J-L Mozos, P. Ordejon, J. Taylor, and K. Stokbro, "Density-functional method for nonequilibrium electron transport," *Phys. Rev. B*, vol. 65, p. 165401, March 2002.
- [9] D. Stradi, U. Martinez, A. Blom, M. Brandbyge, and K. Stokbro, "General atomistic approach for modeling metal-semiconductor interfaces using density functional theory and nonequilibrium Green's function," *Phys. Rev. B*, vol. 93, p. 155302, April 2016.